Insights into the Photodecomposition of Azidomethyl Methyl Sulfide: A S 2 /S 1 Conical Intersection on Nitrene Potential Energy Surfaces Leading to the Formation of S -Methyl- N -sulfenylmethanimine

Manuel Algarra, Juan Soto, Luis Pinto da Silva, M. Soledad Pino-González, J. Enrique Rodríguez-Borges, Joelle Mascetti, Fabien Borget, Adel Reisi-Vanani, Rafael Luque

Insights into the photo-decomposition of azidomethyl methyl sulfide: A S_2/S_1 conical intersection on nitrene potential energy surfaces leads to formation of *S*-methyl-*N*-sulfenylmethanimine

Manuel Algarra,[§,*] Juan Soto,[†,*] Luis Pinto da Silva,[□,‡] M. Soledad Pino-González[Θ], J. Enrique Rodríguez-Borges,[□] Joelle Mascetti,[☼] Fabien Borget,[•] Adel Reisi-Vanani,[▪] Rafael Luque,[#,¥,*]

[§]CQM-Centro de Química da Madeira. Universidade da Madeira, Campus Universitário da Penteada, 9020-105 Funchal, Portugal.

[†]Dept. Physical Chemistry, Faculty of Science, Univ. Málaga, Spain.

[□]Chemistry Research Unit (CIQUP), Department of Chemistry and Biochemistry, Faculty of Sciences of University of Porto, R. Campo Alegre 697, 4169-007 Porto, Portugal.

‡LACOMEPHI, GreenUP, Department of Geosciences, Environment and Territorial Planning, Faculty of Sciences of University of Porto, R. Campo Alegre 697, 4169-007 Porto, Portugal.

[Θ]Dept. Organic Chemistry, Faculty of Science, Univ. Málaga, Spain

[☼]Institut des Sciences Moléculaires, Univ. Bordeaux, Talence. France

[•]Physique des Interactions Ioniques et Moléculaires. Aix Marseille Univ. Marseille. France

[▪]Department of Physical Chemistry, Faculty of Chemistry, University of Kashan, Kashan, Iran

[#]Dept. Organic Chemistry, Univ. Córdoba. Edif. Marie Curie, Ctra N IVa Km 396, 14014, Córdoba, Spain.

¥Peoples Friendship University of Russia (RUDN University), 6 Miklukho Maklaya str., 117198, Moscow, Russia

ABSTRACT: UV photo-decomposition of azidomethyl methylsulfide (AMMS) yields a transient *S*-methylthiaziridine which rapidly evolves to *S*-methyl-*N*-sulfenylmethanimine at 10K. This species was detected by infrared matrix isolation spectroscopy. The mechanism of the photoreaction of AMMS has been investigated by a combined approach, using low temperature matrix isolation FTIR spectroscopy in conjunction with two theoretical methods, namely, complete active space self-consistent field (CASSCF) and multi-configurational second-order perturbation (MS-CASPT2). The key step of the reaction is governed by a S_2/S_1 conical intersection localized in the neighborhood of the singlet nitrene minimum which is formed in the first reaction step of the photolysis, that is, N_2 elimination from AMMS. Full assignment of the observed infrared spectra of AMMS has been carried out based on comparison with DFT and second-order perturbation Møller-Plesset (MP2) methods.

Keywords: CASSCF; MS-CASPT2; Conical Intersection; Intersystem crossing; UV Photochemistry; Matrix Isolation

*Corresponding authors E-mails: manuel.gonzalez@staff.uma.pt (M. Algarra); soto@uma.es (J. Soto) and rafael.luque@uco.es (R. Luque)

INTRODUCTION

Organic azides are energy rich molecules with several industrial and technological applications, known and used since the beginning of the last century. Azides are widely employed in a diversity of synthetic preparations, important components in click chemistry and as nitrogen source due to the facile loss of N_2 upon thermal or photochemical activation.[1-6] They also find applications in fields including the automobile industry (e.g. propellants in air-bag systems of automobiles) and semiconductor processing (as single source precursors of thin films), simplifying synthetic processes for the preparation of such materials.[7-11]

Due to the significant interest of these molecules, numerous spectroscopic studies have targeted the fundamental understanding of decomposition products of organic azides and their intermediates supported by computational analysis. Both thermal and photochemical decomposition of organic azides have been extensively studied in solution and various matrices by photoelectron and FTIR matrix isolation spectroscopies and demonstrated to exhibit highly interesting and complex chemistries.[12-15] Imine derivatives have been observed together with reactive nitrene intermediates under laser flash photolysis.[16-19] Based on these decomposition patterns, various pathways were identified as depicted in Scheme 1. Type 1 pathways[12,13] lead to imines as final products after N_2 loss via nitrene intermediate followed by isomerization. Alternatively, imines may be formed by a 1,2-H shift synchronous with N_2 elimination. Type 2 pathways[14] involve transfer of intra-groups (proton or alkyl) onto the electron-rich N and may involve a cyclic transition state. The thermolysis of azidobenzyl phenyl sulfide has been reported to generate a sulfenylimine product, in which a thiaziridine intermediate was proposed.[20] This type of rearrangement represents the least common rearrangement among those described in literature and can be considered as Type 3 pathway in the present work (Scheme 1). The possible formation of the rearrangement product, according to Type 3 pathway, would be relevant because the obtained *N*-sulfenylimines (*N*-alkylidenesulfenamides)[24,25] are useful intermediates in the syntheses of antibiotics and other bioactive molecules.[26,27] *N*-sulfenylimines have a remarkable reactivity, with possible redox processes at the imine bond (i.e. reduction) and sulfur (i.e. oxidation) as well as nucleophilic additions to the same carbon and electrophilic additions at the nitrogen.

In this work, we aimed to investigate the photochemical decomposition of an organic aliphatic sulfide azide in order to understand the possibilities to couple such decomposition with the generation of interesting light-mediated compounds for organocatalysis.[21] Sulfur-

containing aliphatic azides are attractive since click chemistry applications may allow their use in nanotechnology related fields including functionalization and surface patterning as for other types of azides.[22,23] Aromatic thio-azides have occasionally been described.[18,20] but to the best of our knowledge, this is the first reported mechanistic study related to alkyl thio-azides that combine matrix isolation techniques and computational calculations.

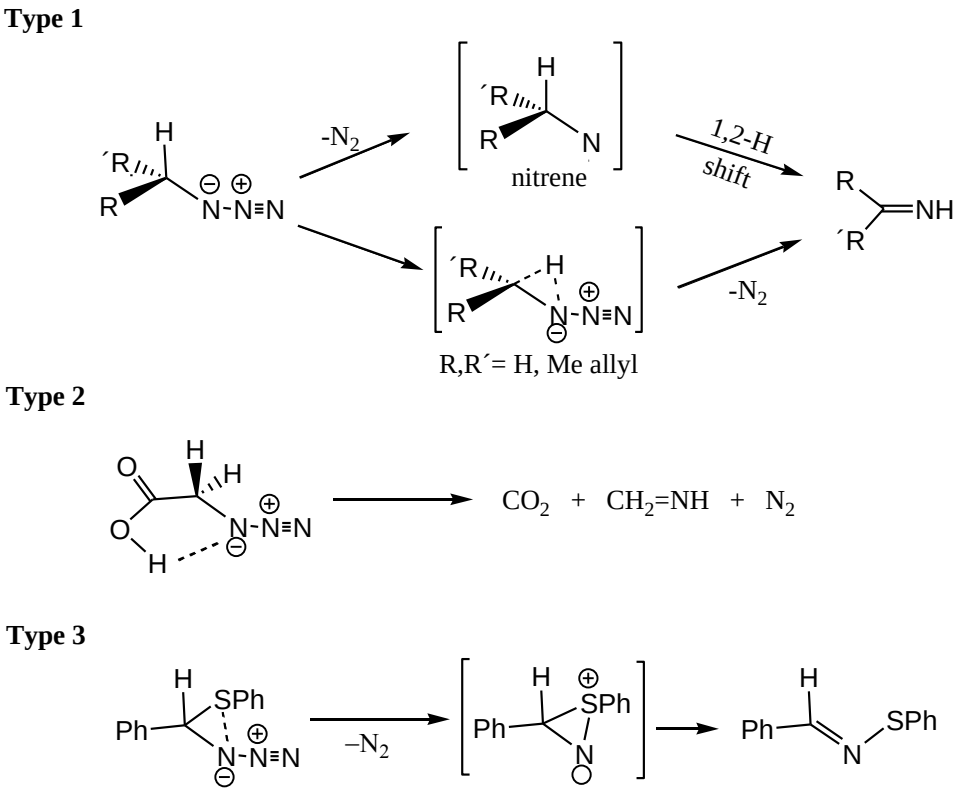

Scheme 1. Different pathways in the thermic decomposition of aliphatic azides

RESULTS AND DISCUSSION

With the aim to elucidate the decomposition mechanism of azidomethyl methylsulfide (AMMS), the method of matrix isolation infrared spectroscopy was used in these studies together theoretical calculations.

UV photodecomposition of AMMS. AMMS was irradiated under UV light, see Supporting Information (SI) details of the UV spectra of AMMS (Figure S1A) and the emission spectra of the used Hg lamp, (low pressure Hg lamp irradiating above 180 nm (Figure S1B). Isolation in Ar, N_2 and Xe matrices at 10K were recorded for the first time in order to estimate energy differences, barriers of inter-conversion and vibrational spectra of the different conformers of AMMS. Annealing of the matrices was also systematically carried out.

Pure AMMS was characterized by recording FTIR spectra in N_2, Ar and Xe matrices at 10 K. Figure 1A displays the spectra of AMMS in Ar matrix (2040-2180 cm^{-1}) showing an excellent quality spectrum with sharp absorption bands as compared to those under Xe or N_2, where less matrix site effects are observed. In this spectral region are localized the bands corresponding to the asymmetric mode $\nu_a(N_3)$ of the pattern molecule, in fact, at least six intense bands are recorded at 2115, 2118, 2122, 2127, 2130 and 2134 cm^{-1} (Tables 1 and S1). The correlation between the calculated and observed bands is not straightforward. Furthermore, it is well known that some azides, e.g., methyl azide, give intense overtones and combination bands in this spectral region, which are more intense than the fundamental modes that originate them.[28,29] Thus, we cannot assign all the observed bands in the ~2100 cm^{-1} region to fundamental modes. Furthermore, for example, isomers 2 and 5 (Table 1 and Figure S2) have the same electronic energy and their fundamental frequencies are almost the same. Hence, we would expect to observe only five bands in this region of the infrared spectra. Therefore, we assume that the former six bands arise from five fundamental frequencies plus one combination band. Vibrational analysis in internal coordinates for isomer 3 (C_s conformer) is given in Tables S2 to S5.

In the temperature range 10-30K, the energy barriers between all conformers are too high (between 1 and 3 kcal/mol according to our DFT calculations) to allow interconversion processes. Only few changes related to metastable matrix site vanishing could be observed. Table 1 lists the bands, which were observed in Ar matrix at 10 K and the calculated ones by MP2, of the most characteristic functional groups for the isomers of AMMS. The asymmetric stretching frequency of -NNN group, predicted for all conformers, lies in the region 2156-2166 cm^{-1}. The experimental spectrum reveals, as previously mentioned six bands, strongest bands which are extending from 2115-2134 cm^{-1} (Figure 1A). As it has been previously reported,[30] the bands show asymmetric shapes, additional splitting, and an appreciable change in the intensities from matrix to matrix.

Table 1. Experimental (in Ar 10K) and calculated frequencies (MP2/def2-QZVPP) of the vibrational modes of *AMMS* isomers

AMMS1[a]	AMMS2	AMMS3	AMMS4	AMMS5	AMMS6	(Ar 10K)	Assignment[b,c]
2311	2301	2320	2305	2301	2308	2115/2118/2122/ 2127/2130/ 2134 s	$\nu_{as}(N_3)$
1346	1342	1323	1341	1342	1355	1313	$0.2\nu(CN)+0.7\nu_s(N_3)$
1283	1272	1310	1284	1271	1267	1245/1220 s	$0.9\delta_{rock}(CH_2)$
1245	1238	1191	1218	1238	1247		$0.9\delta_{twi}(CH_2)$
1026	1025	1013	1004	1025	1025	1003	$0.1\nu(CN)+0.7\delta_{rock}(CH_3)$
980	987	992	990	987	987	959	$0.1\delta_{wag}(CH_2)+0.8\delta'_{rock}(CH_3)$
721	726	756	748	726	729	697/694/684	$\nu(CS)$
687	689	657	694	689	681	654/655/659	$0.1\nu'(CS)+0.2\delta(CNN)+0.6\delta(NNN)$

[a]Labelling of isomers according to Figure S1. [b]Assignment according to vibrational potential energy distribution in internal coordinates of the AMMS3 isomer (Cs symmetry). [c]Definition of internal coordinates given in Table S2A and atom numbering for vibrational analysis in Figure S3.

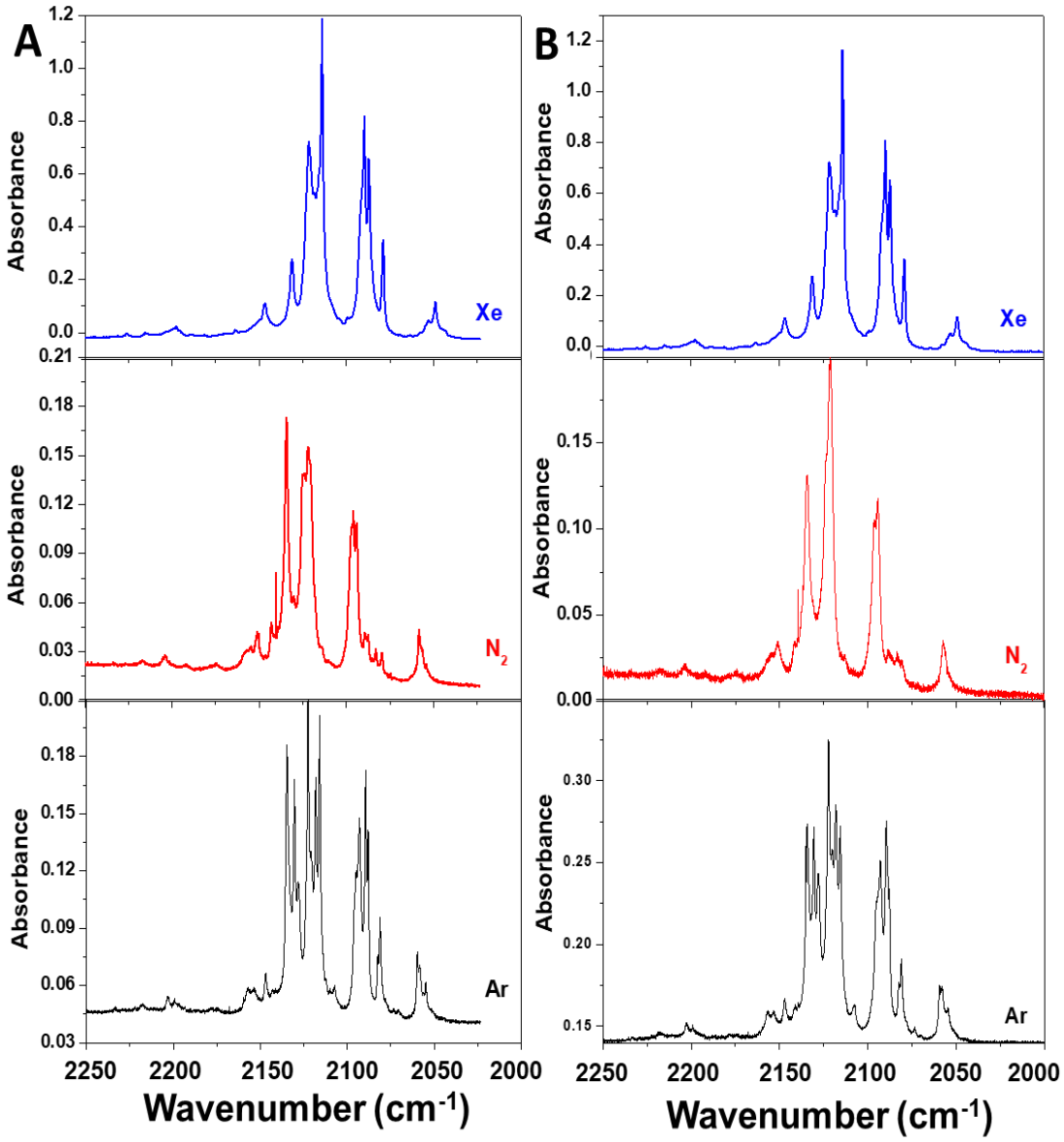

Figure 1. FTIR spectra in Ar, N_2 and Xe matrix (2000-2300 cm^{-1} spectral range) of (**A**) Trapped AMMS recorded at 10K. (**B**) Annealing of AMMS at 30K recorded at 10K

The presence of conformers and matrix site effects are also present for other vibrational modes (Figures S3-S4): CH_2 and CH_3 bending modes (1420-1450 cm^{-1}), CH_2 and CH_3 rocking modes (around 860 and 905 cm^{-1}). Bands located in the 1200-1240 cm^{-1} range can be assigned to $\delta_{rock}(CH_2)$ and $\delta_{twi}(CH_2)$ modes. The recorded spectra were too noisy to observe weak bands below 800 cm^{-1}, which could correspond to deformations of NCH and NCS moieties. Spectra recorded in solid N_2 exhibited less bands as compared to that on Ar, with some missing weak bands. Table S1 summarizes all annealed experiments in N_2 matrices. These findings may indicate slightly lower barriers between conformers under N_2 as compared to Ar which could be related to low affinities of AMMS to form a well-defined local crystalline structure resulting in poorly defined sites, with a wide range of local geometries (matrix site effect, $\Delta\nu < 10$ cm^{-1}, Figure S5).

After deposition, the matrix was subjected to a step-by-step annealing procedure (from 10 to 30K in Ar, Figure 2B), aiming to alter relative conformer populations to further support the interpretation of the experimental spectra. In Ar, the observed spectral changes were found to be minor and essentially ascribable to site conversion. Annealing experiments in N_2 were comparatively more informative (Figure S6), with six remaining bands at 2122(s), 2135(m), 2151(w), 2081(w), 2057(w) and 2095(ms) cm^{-1}, respectively, correlated to the $\nu_{as}(N_3)$ vibration of the azide group. Interestingly, a change in temperature generated intensity changes between bands at 2135 cm^{-1} (increasing when decreasing T) and 2122 cm^{-1} (increasing with T).

The photochemical decomposition of AMMS was subsequently conducted under UV-visible light and studied by FTIR in Ar-matrix (10 K) at different times of irradiation (typically 0-120 min). After 10 min irradiation, IR vibrations of $\nu_{as}(N_3)$ and $\nu_s(N_3)$ at 2100-2200 cm^{-1} (Figure 2A) and 1180-1260 cm^{-1} (Figure 2B) started to disappear, while many new features due to photodecomposition products are growing. New peaks of increasing intensity were observed after 90-120 minutes of irradiation in the 2800-3300 cm^{-1} (Figure 2C) region (namely 2850, 2875, 2948, 3012, 3165, 3169, 3174, 3189, 3233, 3239 and 3293 cm^{-1}, (Figures S7 and S8). Clearly, these bands arise from of a new compound formed in the photolysis of the parent azide and could be assigned respectively to the stretching modes of the $=CH_2$ and $-CH_3$ moieties of such a new compound. In addition, new weak bands are observed in the range 682-748 cm^{-1} (Figure 2D).

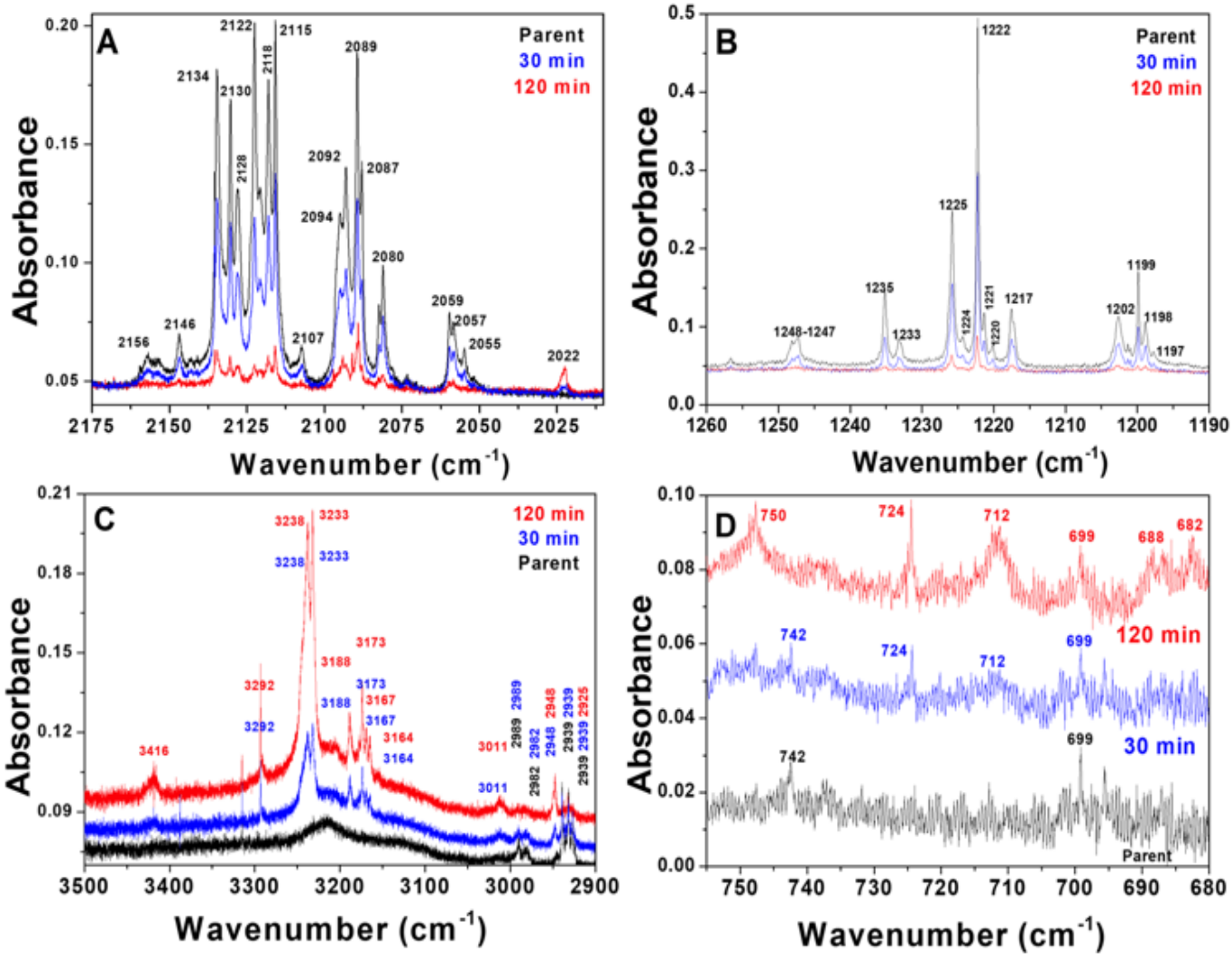

Figure 2. FTIR spectra obtained after deposition of AMMS in Ar at 10K (black) and after irradiation under UV light for 30 min (blue) and 120 min (red), showing the decrease of all AMMS bands and the growing of new bands in the 3300-3100 and 760-680 cm^{-1} regions.

Infrared absorption bands of the H_2C=N- moiety. The most featuring bands that are registered in the spectra depicted in Figure 2 correspond to two bands that appear in the 3100-3200 cm^{-1} region (Figure 2), whose intensities increase as time increases. In addition, it is observed that such absorption bands depend strongly on the supporting matrix and the material phase in which the spectra are registered, Figure S9 and Table 2, respectively. The infrared spectra of the parent molecule, methanimine (H_2C=NH), show the same behavior for the asymmetric stretching mode of CH_2. Table 2 collects the positions of the bands of methanimine calculated in this work and those ones given by one of us (FB)[31] and other two independent groups.[32,33] The most striking data of this table refers to the C-H stretching mode of the H_2C=N- moiety, which varies in both position and intensity as vary

the experimental conditions. Therefore, we have assigned these two bands to the asymmetric stretching of CH_2= (3238 cm^{-1}) and $\nu_s(CH_2)/\nu'_{as}(CH_3)$ (3233 cm^{-1}) modes of *S*-methyl-*N*-sulfenylmethanimine, respectively, which are calculated at these wavenumbers (Table S3A-B).

Table 2. Infrared absorption bands (in cm^{-1}) of methanimine (observed and calculated)

	Ar (10K)[a]	Ar (4K)[b]	Gas[c]	Calc.[d]	Assignment[e]
ν_1	3266	-	3264	3493 vw (*0.93*)[f]	ν(NH)
ν_2	3162/3140	3035 m	3038	3203 m-s (*0.95*)	$\nu_{as}(CH_2)$
$\nu_4+\nu_6$		2966 w-m	-		
ν_3	2987/2916/2886	2926 s	2915	3093 s (*0.94*)	$\nu_s(CH_2)$
ν_4	1642	1641 s	1638	1678 m-s (*0.98*)	$0.7\nu(CN)+0.3\delta_s(CH_2)$
ν_5	1411	1453 s	1453	1492 m (*0.97*)	$0.3\nu(CN)+0.7\delta_s(CH_2)$
ν_6		1348 s-vs	(1342)[g]	1371 vs (*0.98*)	$0.6\delta(HNC)+0.4\delta_{rock}(CH_2)$
ν_7	1186	1059 vs	(1055)[h]	1073 vs (*0.98*)	$0.4\delta(HNC)+0.6\delta_{rock}(CH_2)$
ν_8	1117	1123 vs	1131	1171 vs (*0.97*)	Γ(CN)
ν_9		1063 s	1058	1098 s (*0.96*)	$\gamma(CH_2)$

[a]Ref. 31. [b]Ref. 32. [c]Ref. 33. [d]MP2/def2-QZVPP, this work. [e]Assignment according to the potential energy distribution obtained from the ***GF*** vibrational analysis and definition of internal coordinates given in Table S5. [f]In parenthesis ratio: [observed (gas phase)/calculated]. [g]Approximate value of the central minimum. [h]Average of the multiple peaks.

Theoretical study of the reaction mechanisms. Scheme 2 proposes a reaction mechanism for the formation of *S*-Methyl-*N*-sulfenylmethanimine after AMMS photodecomposition. Thus, according to the mechanism proposed in Scheme 2, to study the photodecomposition reaction, we have applied the CASSCF and MS-CASPT2 methods[34,35] in conjunction with the ANO-RCC basis sets[36,37] as implemented in the MOLCAS 8.2 program.[38] Table 3 collects the vertical transition energies of the electronic transitions calculated at the MS-CASPT2 level. The assignment of electronic transitions given in Table 3 is based on the state average CASSCF orbitals of the minimum energy geometry of AMMS given in Figure S10. According to the calculated excitation energies, upon exposition to UV-radiation, the S_1 state of AMMS is populated (Table 3), the next state is out of the range of the source applied.

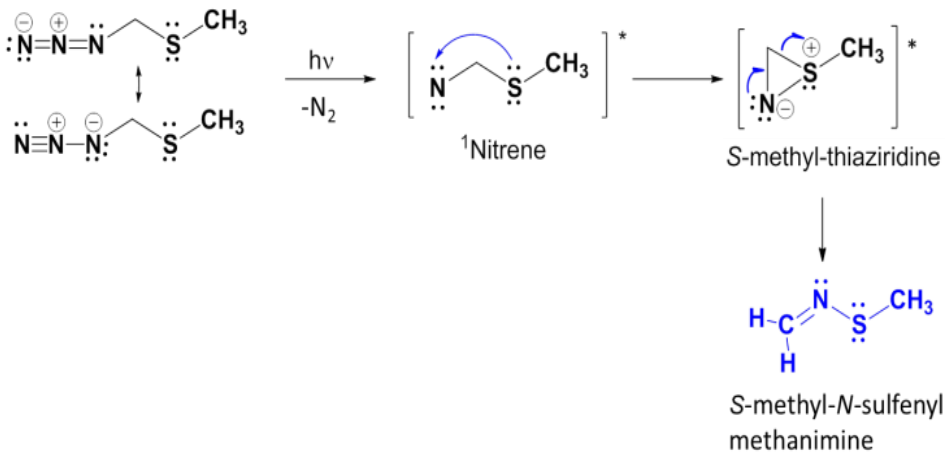

Scheme 2. Schematic representation of the proposed photochemical decomposition of AMMS.

Given that the first step in the decomposition of azide derivatives[39-42] usually gives the corresponding nitrene plus N_2, we have built the linear interpolation[43-51] that connects the S_0 minimum of the azide derivative (M_0, Figure 3(a)1)) with its dissociation products (Figure 3b). The potential energy profile depicted in this figure indicates that there would be two stationary points on the S_1 (1^1A") surface around the Franck-Condon point, that is, a minimum and a transition state. In fact, we have been able to optimize these stationary points, denoted as M_1 (Figure 3(a)2) and TS_1 (Figure 3(a)3), respectively. TS_1 is located at only ~14 kcal/mol with respect to M_1 and ~33 kcal/mol below the vertical excitation of the minimum ground state (M_0). In consequence, after surmounting a small energy barrier on the S_1 surface, AMMS dissociates into N_2 (S_0) and nitrene on the lowest singlet surface by decaying through a conical intersection (CI_1, Figure 3(a)4). Therefore, the nitrene species would be generated in its lowest singlet state, which is an open shell structure (S_1, 1^1A", under C_s symmetry) with two unpaired electrons localized in the *p*-type orbitals of the N atom. At the CASSCF level, we have found a minimum on the 1^1A" surface of the nitrene species (M_2, Figure 4(b)) which lies 32 kcal/mol above its triplet ground state (T_0, 1^3A", Figure 4(a)). In contrast, the vertical excitation energy of M_2 to its first excited singlet (S_2, 1^1A', Figure S4(c)) amounts only to ~0.1 kcal/mol, which indicates that both singlet states of the nitrene derivative are strongly coupled. Interestingly, we have optimized a S_2/S_1 conical intersection[52] (CI_2, Figure 4(d)), which is located at the proximity of the minimum of M_2. It must be remarked that it is a conical intersection what efficiently couples/decouples two electronic states. Furthermore, the analysis of the branching space defined by the gradient difference and derivative coupling vectors given in Figure 4(d) suggests that internal conversion through this conical intersection leads to formation of *S*-

methylthiaziridine. Therefore, in order to confirm the mechanism proposed in Scheme 2, we have computed the profiles of the potential energy surfaces (Figure 5), which leads from nitrene (CH_3SCH_2N, Figure 4(b)) to *N*-sulfenylimine ($CH_3S\text{-}N{=}CH_2$, Figure 4(g)) passing by the aziridine intermediate (Figure 4(e)). It is observed in this figure that the path through the CI_2 conical intersection is barrierless. Once the *S*-methylthiaziridine intermediate is formed, the rearrangement to *N*-sulfenylimine needs to surmount an energy barrier. Due to the optimized transition state (TS_3, Figure 4(f)) is 34 kcal/mol below the starting point (nitrene, M_2), the reaction can advance to *N*-sulfenylimine formation. To avoid any type of confusion to the reader, it should be note that the value of 34 kcal/mol mentioned above corresponds to the true optimized geometry, the point indicated in Figure 5 corresponds to the starting point (~14 kcal/mol below M_2) in the search for the true transition geometry. The state-average active space that has been used in these interpolations is given in Figure S14.

Table 3. Vertical excitation energies in eV of the singlet states of AMMS (C_s, MS-CASPT2)[a,b]

Transition	ΔE(eV)	OS[c]	Configuration[d]
1A'→ 2A'	6.02	0.0085	46% $n_\pi(NN)^1\pi^*(NNN)^1$ 40% $n_\sigma(NN)^1\pi^*(NNN)^1$
1A'→ 3A'	7.71	0.0040	82% $p_\pi(S)^1\pi^*(NNN)^1$
1A'→ 4A'	8.40	0.5209	25% $n_\pi(NN)^1\pi^*(NNN)^1$ 44% $n_\sigma(NN)^1\pi^*(NNN)^1$
1A'→ 1A"	4.57	0.0009	89% $n_\pi(NN)^1\pi_\sigma^*(NN)^1$
1A'→ 2A"	6.47	0.0001	92% $p_\pi(S)^1\pi_\sigma^*(NN)^1$
1A'→ 3A"	7.40	0.0054	90% $n_\sigma(NN)^1\pi_\sigma^*(NN)^1$
1A'→ 4A"	10.11	0.0017	61%$\pi(NNN)^1\pi_\sigma^*(NN)^1$ 18% $n_\pi(NN)^0\pi^*(NNN)^1\pi_\sigma^*(NN)^1$

[a]C_s optimized geometry. [b]Four state average CASSCF wavefunction, IPEA=0.25, Imaginary shift = 0.1. [c]Oscillator strength. [d]MS-CASPT2 main electronic configurations of the excited states referred to the ground state configuration (see text). Only contributions with weight greater than 15% are included.

Despite *S*-methyl- *N*-sulfenylimine formation is not clearly observed in the experiments, the band registered at 3416 cm^{-1} (Figure 2C) could be assigned to the ν(NH) mode the imine. Therefore, we have searched for the reaction channel that would lead to this compound. The potential energy profiles of the interpolations are represented in Figure 6. The reaction path on the lowest energy surface is almost barrierless, the optimized

transition state at the CASSCF level for this process (TS_4, Figure 4(h)) lies only ~1 kcal/mol above of the singlet nitrene minimum (M_2).

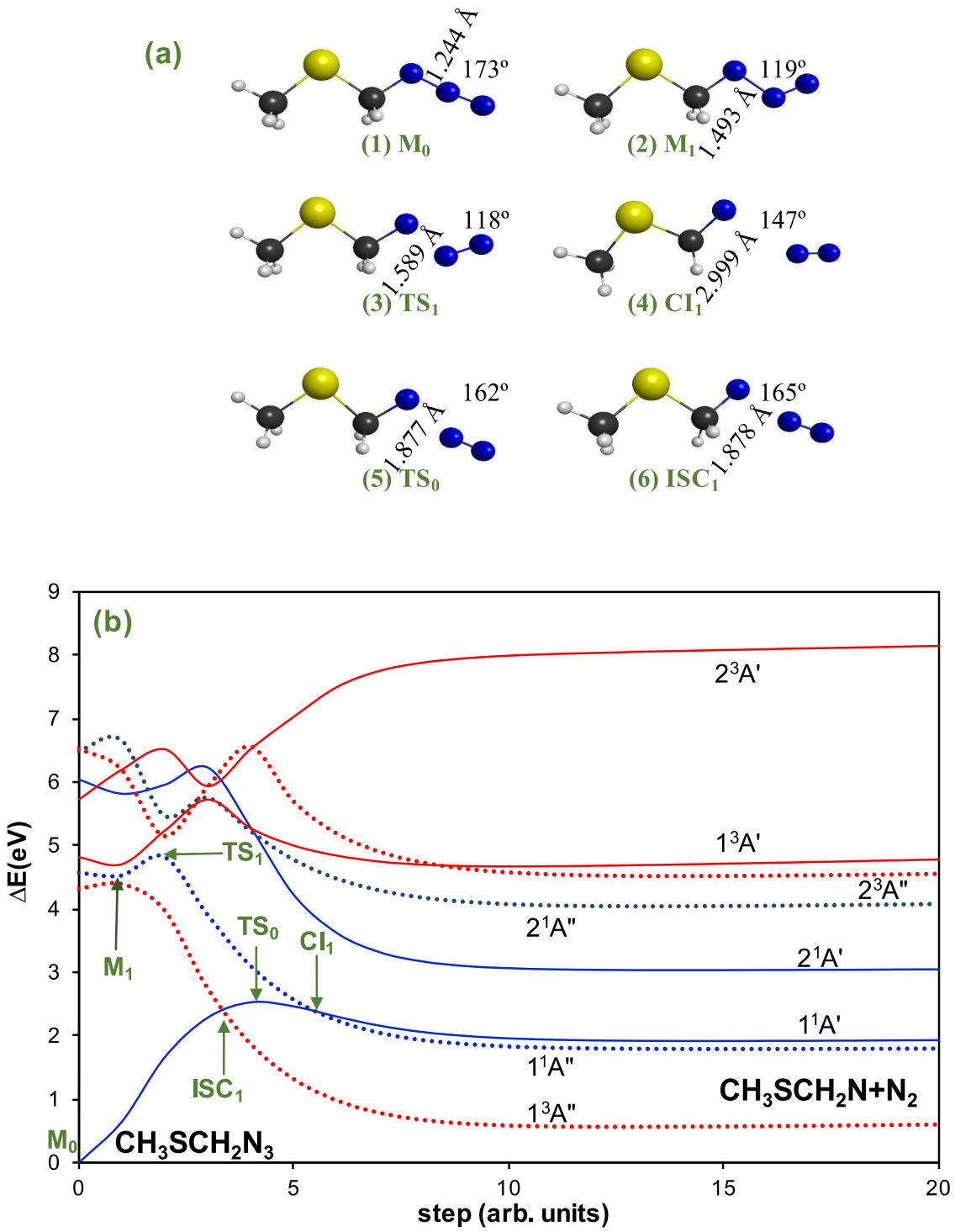

Figure 3. (a) CASSCF/ANO-RCC geometries of the critical points in the thermal and photochemical decomposition of the azide. **(b)** MS-CASPT2/ANO-RCC profiles of the lowest potential energy surfaces for dissociation of azidomethyl methylsulfide into nitrene and N_2. SA-CASSCF reference wavefunction: 16 electrons distributed in 12 orbitals; four roots in each symmetry species (C_s). State symmetry: blue solid: ^{1}A'; blue dotted: ^{1}A"; red solid: ^{3}A'; red dotted: ^{3}A".

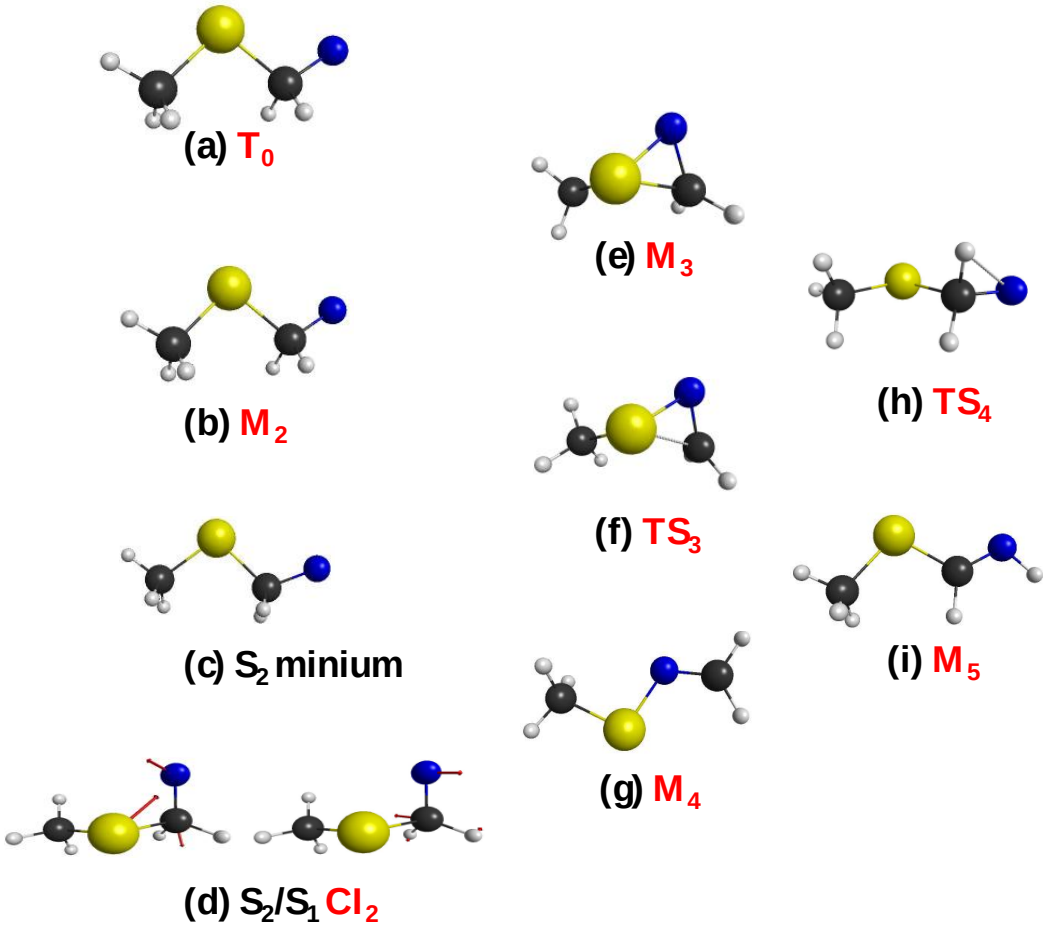

Figure 4. CASSCF (14e,13o)/ANO-RCC optimized geometries of the species involved on the reactions after N_2 elimination of the parent azide: (a) T_0 triplet minimum (1^3A"); (b) S_1 singlet minimum (1^1A"); (c) S_2 singlet minimum (1^1A'); (d) two views of the S_2/S_1 conical intersection CI_2: **left**: gradient difference vector; **right:** derivative coupling vector; (e) M_3 *S*-methylthiaziridine; (f) TS_3 transition state; (g) M_4 *N*-sulfenylimine; (h) TS_4 transition state; (i) M_5 imine.

Therefore, in principle, formation of the imine derivative would be energetically accessible. In consequence, if it is not clearly observed it must be concluded that formation of this species is hindered by some process. The only reason that we have found to explain why is not experimentally observed is the *CI*$_2$ conical intersection in the proximity of the nitrene that was formed in the first reaction step from the parent azide. This conical intersection acts as an attractor that guides the system to it and decouples the S_2 and S_1 states of nitrene leading, in turn, the system to the amine channel instead of the imine path. Thus, we can postulate that is a dynamic effect what favors yielding of the amine instead of the imine derivative.

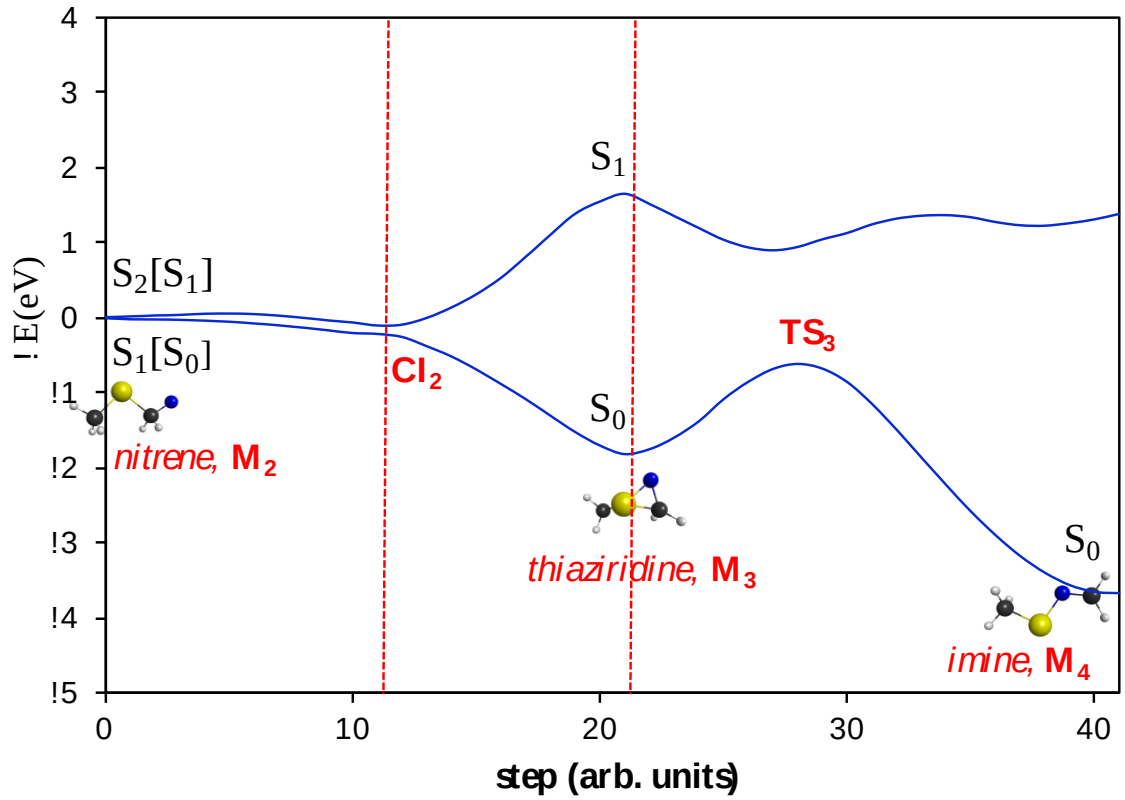

Figure 5. MS-CASPT2/ANO-RCC profile along the interpolation line connecting (1^1A") nitrene with CH_3SNCH_2. C_1 state average (four states) CASSCF reference wavefunction. 14 electrons distributed in 13 orbitals. $S_i[S_j]$ on the left side of the graphic indicates the notation of the electronic state at the nitrene minimum M_2 (S_i) and at the final product M_4 (S_j).

Concerning thermal dissociation of AMMS, starting at the ground state surface, the interpolation line suggests that there is a transition state (TS_0) on the S_0 surface and a T_1/S_0 intersystem crossing (ISC_1) between the ground and lowest triplet states. In fact, these two points were optimized on the low-lying potential energy surfaces to demonstrate the reliability of our interpolation method. The structures and energetic of these critical points are given in Figure 7(a). Both TS_0 and ISC_1 yield nitrene and molecular nitrogen, the path through TS_0 leads to formation of (1^1A') singlet nitrene and the channel through ISC_1 generates (1^3A") triplet nitrene, in accordance with previous studies.[53-55] Unfortunately, triplet nitrene has not been observed in our experiments. The detection of triplet species would require, for example, EPR spectroscopy, that has been successfully applied to other nitrene derivatives.[56-58] However, the calculations point out that formation of this species in the thermal decomposition of the azide is highly probable. Two factors reinforce the above assertion:[59] (i) the magnitude of calculated spin orbit coupling constant for the crossing point that amounts to 40 cm^{-1}; (ii) the geometrical distance between the calculated geometries of TS_0 and ISC_1 is only 0.05 Å.

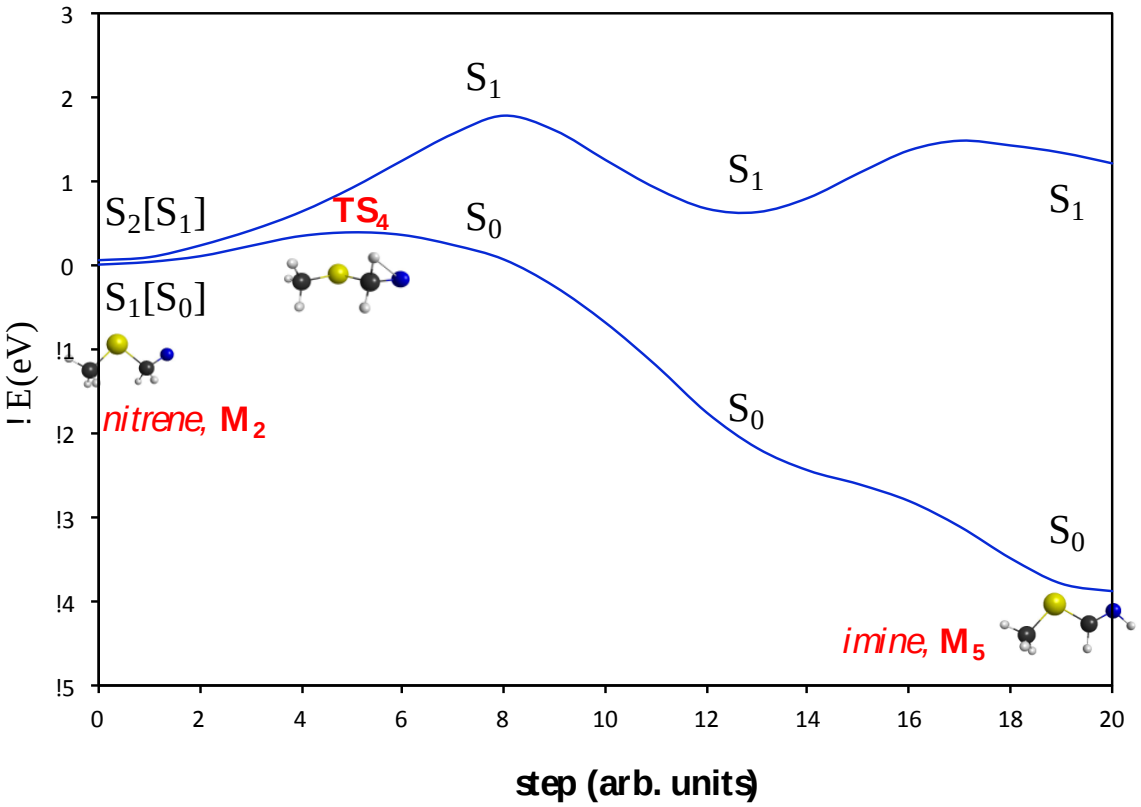

Figure 6. MS-CASPT2/ANO-RCC energy profiles along the interpolation line connecting $1^1A''$ S_1 nitrene with CH_3SCHNH. C_1 state average (four states) CASSCF reference wavefunction. 14 electrons distributed in 13 orbitals. $S_i[S_j]$ on the left side of the graphic indicates the notation of the electronic state at the nitrene minimum M_2 (S_i) or at the final product M_5 (S_j).

CONCLUSIONS

In conclusion, the present work studies the decomposition of AMMS upon UV irradiation. The general picture of the reaction mechanisms is given in Figure 7. It is proposed that the main product of the photoreaction is *S*-methyl-*N*-sulfenylmethanime. An analogous reaction has been recently reported by Wentrup *et. al.* for the photolysis of trimethylsilyl azide which gives *N*-(dimethylsilyl)-methanimine.[56]

FTIR spectra in Ar matrix are more complex because of presence of site effects; the nature of matrix plays an important role in the intensity and positions of the bands and in the inter-conversion mechanisms between the different conformers. The main fingerprint found to confirm the presence of *S*-Methyl-*N*-sulfenylmethanimine was the emerging bands at 3175 and 3190 cm^{-1}; and the doublet 3230 and 3237 cm^{-1}

observed after irradiation, assigned to the -N=CH_2 moiety of this organic compound. The calculations on the reaction mechanism demonstrate that a S_2/S_1 conical intersection in the seam of crossing of the S_2 and S_1 states of nitrene, which is localized in the proximity of S_1 minimum of nitrene, governs the reaction mechanism after N_2 elimination in the first step of the photochemical decomposition.

To finish, rearrangement in the excited states (RIES), such as cyclization or hydrogen migration [see e. g. Refs. 60-68], are processes that are not considered in this work because the excitation energy at the Franck-Condon geometry, which populates the S_1 state, is well above the minimum (M_1) on the S_1 surface (Figure 7(a)). In consequence, after absorption of one photon, the system gains enough internal energy to surmount a small barrier which will lead to N_2 elimination, forming the nitrene species in its lowest singlet state (S_1, 1^1A"). In addition, once singlet nitrene is formed, it decays through a reaction channel that no needs extra energy to reach the final product, that is, *S*-methyl-*N*-sulfenylmethanime (Figure 7(b)).

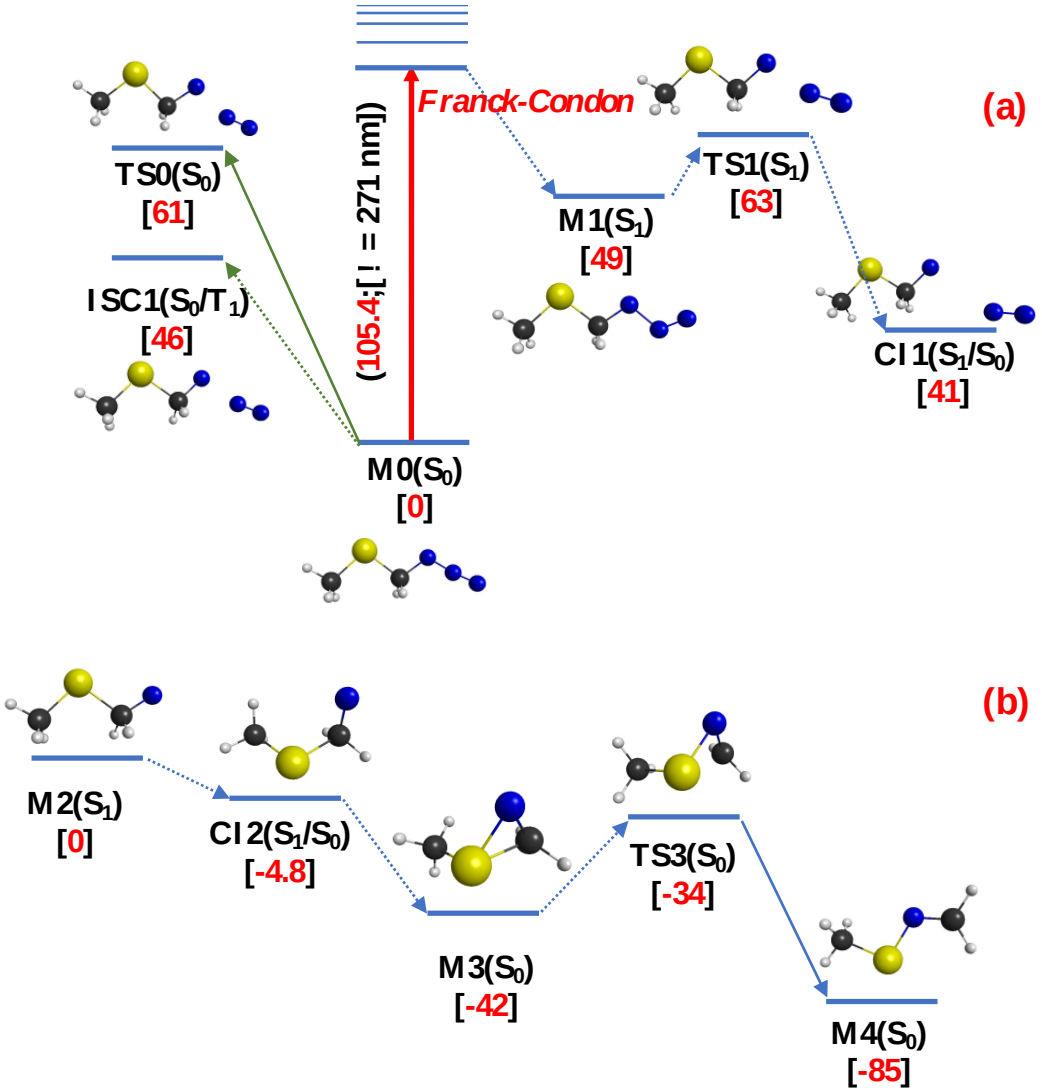

Figure 7. MS-CAST2/ANO-RCC schematic representation of the reaction mechanisms leading to formation of (**a**) singlet nitrene and triplet nitrene (**b**) *S*- Methyl-*N*-sulfenylmethanimine. In square bracket, energy in kcal/mol.

EXPERIMENTAL SECTION

Chemicals. Sodium azide (NaN_3), and chloromethyl methyl sulfide, were purchased from Sigma-Aldrich and used without further purification. Acetonitrile previously treated to get it in anhydrous conditions was obtained from Merck. ^{1}H,^{13}C NMR (300 MHz) spectrum was recorded in a Bruker WM spectrometer, using TMS as the internal reference (chemical shifts in δ values, J in Hz). Mass spectra were recorded on a Kratos MS-59 spectrometer. Microanalysis was performed in a Perkin-Elmer 240B element analyzer.

Synthesis of Azidomethyl methyl sulfide (AMMS)*. Following previously synthesis procedures was synthesized AMMS, with several modifications.[69-71] A mixture of chloromethyl methyl sulfide (1.15 g, 1.0 mL, 11.3 mmol), NaN_3 (1.1 g, 17 mmol) and

tetrabutylammonium iodide (406 mg, 1.1 mmol) in CH_3CN/H_2O 1:1 (30 mL) was stirred under Ar atmosphere for 2 days at 45 ºC. The reaction mixture could reach room temperature and Et_2O (100 mL) and H_2O (100 mL) were added. The organic layer was separated and washed with brine (2×100 mL). The organic extract was dried over Na_2SO_4 and filtrated. The solvent was removed under vacuum and the corresponding pure AMMS was obtained as a yellowish liquid (1.11 g, yield 95%) which absorbed at 298 nm (Figure S1). We confirmed the purity of these samples through NMR, the obtained spectra showed AMMS and traces of ethyl ether: ^{1}H NMR ($CDCl_3$): δ = 4.22 (*s*, 3H, S-C**H**$_3$); 2.25 (*s*, 2H, S-C**H**$_2$N$_3$) (Figure S15); ^{13}C NMR ($CDCl_3$): δ= 15.23(**C**H$_3$); 55.92 (**C**H$_2$); *Anal.: cal.* For $C_2H_5N_3S$: C: 23.29 %; H: 4.89 %; N: 40.74 %; S: 31.09 %. Found: C: 23.31 %; H: 4.92 %; N: 40.71 5; and S: 31.04 %. A parent peak at 103 a.m.u. was observed on the 70 e.V. electron impact mass spectrometry. *(Care was taken to ensure good ventilation due to the formation of toxic HN_3.)

FT- IR Matrix Isolation Spectroscopy. The experimental techniques used to obtain Ar and N_2 matrices have been described elsewhere.[72] The pre-mixed organic azide vapors with Ar and N_2 matrix gases were prepared at room temperature using standard manometric techniques with concentrations of 1:900 for all experiments*****. Samples were continuously deposited onto a copper plate cooled down at 20 K. A FTIR spectrometer Nicolet series II Magna system 750 was used to record the spectra of samples cooled at 10 K by reflectance in the range 550-4000 cm^{-1} with a resolution of 0.125 cm^{-1}. The spectra were recorded immediately after deposition, after annealing of the samples, and after irradiation of the matrices with an OSRAM® 200W high pressure Hg lamp equipped with a quartz envelope (all bands). Deposits were irradiated at 10K with a mercury lamp (λ > 200 nm, average power 150 mW, total fluence: 0.72 $J.m^{-2}$).

COMPUTATIONAL SECTION

CASSCF and MS-CASPT2 calculations. The contraction scheme applied to the ANO-RCC basis sets was (S)[5*s*4*p*3*d*2*f*1*g*]/(C,N)[4*s*3*p*2*d*1*f*]/(H)[3*s*2*p*1*d*]. MS-CASPT2 calculations were performed on top the CASSCF optimized geometries (minima, transition states, conical intersections and intersystem crossings). The standard empirical correction IPEA (0.25) was used in the MS-CASPT2 calculations in conjunction with an imaginary shift of 0.1 to avoid inclusion of intruder states. Spin-orbit coupling constant was

computed with a spin-orbit Fock-type Hamiltonian.[73-77] The active spaces that have been selected for each reaction have been carefully chosen to avoid erroneous answers.[78-80] The analysis of molecular orbitals, geometries and vibrational frequencies have been performed with the programs Gabedit,[81] Molden[82] and MacMolplt.[83] The vibrational analysis in internal coordinates[84] have been performed with the **GF** theory of Wilson[85] and the assignments of the fundamental modes have been done with the help of the vibrational potential energy distribution[86] with computational programs implemented by one of us (JS).[87,88]

DFT and MP2 calculations. The potential energy surface (PES) of AMMS has been investigated with the B3LYP[89,90] hybrid functional and the 6-31G(d) basis sets.[91] Frequencies calculations were performed with the were optimized with the second order Møller-Plesset perturbation (MP2) method[92] and the def2-QZVPP basis sets[93,94] allowing the assignment of these stationary points as true minima and the determination of the corresponding vibrational spectra. All DFT and MP2 calculations were carried out with the GAUSSIAN 16 program.[95]

Supporting Information

Information related to the computational calculations are included here.

AUTHOR INFORMATION

manuel.gonzalez@staff.uma.pt (M. Algarra)
soto@uma.es (J. Soto)
rafael.luque@uco.es (R. Luque)

ACKNOWLEDGEMENTS

MA thanks also This work was supported by FCT-Fundação para a Ciência e a Tecnologia through the CQM Base Fund - UIDB/00674/2020, and Programmatic Fund - UIDP/00674/2020, and by ARDITI-Agência Regional para o Desenvolvimento da Investigação Tecnologia e Inovação, through the project M1420-01-0145-FEDER-000005 - Centro de Química da Madeira - CQM+ (Madeira 14-20 Program). JS thanks Rafael Larrosa and Darío Guerrero for the technical support in running the calculations and the SCBI (Supercomputer and Bioinformatics) center of the University of Málaga for computer resources and projects CTQ2015-65816-R and UMA18-FEDERJA-049. LPS acknowledges funding from FCT under the Scientific Employment Stimulus (CEECIND/01425/2017). The publication has been prepared with support from RUDN University Program 5-100. Fellowship obtained from Gulbenkian Foundation is acknowledged.

REFERENCES

(1) Wentrup, C. Flash Vacuum Pyrolysis of Azides, Triazoles, and Tetrazoles. *Chem. Rev.*, **2017**, *117*, 4562-4623.
(2) Moses, J. E.; Moorhouse. A. D. The growing applications of click chemistry. *Chem. Soc. Rev.* **2007**, *36*, 1249-1262.
(3) Wentrup, C. Carbenes and Nitrenes: Recent Developments in Fundamental Chemistry. *Angew. Chem. Int. Ed.* **2018**, *57*, 11508-11521.
(4) Liu, Q.; Qin, Y.; Lu, Y.; Wentrup, C.; Zeng, X. Spectroscopic Characterization of Nicotinoyl and Isonicotinoyl Nitrenes and the Photointerconversion of 4‑Pyridylnitrene with Diazacycloheptatetraene. *J. Phys. Chem. A* **2019**, *123*, 3793-3801.
(5) Silva, P. J.; Bernardo, C. E. P. Influence of Alkyne and Azide Substituents on the Choice of the Reaction Mechanism of the Cu+‑Catalyzed Addition of Azides to Iodoalkynes. *J. Phys. Chem. A* **2018**, *122*, 7497-7507.
(6) Meisner, Q. J.; Accardo, J. V.; Hu, G.; Clark, R. J.; Jiang, D.; Zhu, L. Fluorescence of Hydroxyphenyl-Substituted “Click” Triazoles. *J. Phys. Chem. A* **2018**, *122*, 2956-2973.
(7) Liu, L. H.; Yan, M. Perfluorophenyl Azides: New Applications in Surface Functionalization and Nanomaterial Synthesis. *Acc. Chem. Res.* **2010**, *43*, 1434-1443.
(8) Lowe, A. B. Thiol-yne 'click'/coupling chemistry and recent applications in polymer and materials synthesis and modification. *Polymer* **2014**, *55*, 5517-5549.
(9) Hiki, S.; Kataoka, K. Versatile and Selective Synthesis of "Click Chemistry" Compatible Heterobifunctional Poly(ethylene glycol)s Possessing Azide and Alkyne Functionalities. *Bioconjugate Chem.* **2010**, *21*, 248-254.
(10) Yurtsever, E.; Calvo, F. Quantum Chemical View on the Growth Mechanisms of Odd-Sized Nitrogen Cluster Anions. *J. Phys. Chem. A* **2019**, *123*, 202-209.
(11) Bera, A.; Bagchi, D.; S. K.; Pal, Improvement of Photostability and NIR Activity of Cyanine Dye through Nanohybrid Formation: Key Information from Ultrafast Dynamical Studies. *J. Phys. Chem. A* **2019**, *123*, 7550-7557.
(12) Dyke, J. M.; Levita, G.; Morris, A.; Ogden, J. S.; Dias, A. A.; Algarra, M.; Santos, J. P.; Costa, M. L.; Rodrigues, P.; Barros, M. T. A study of the thermal decomposition of 2-azidoacetamide by ultraviolet photoelectron spectroscopy and matrix-isolation infrared spectroscopy: Identification of the imine intermediate H2NCOCHNH. *J. Phys. Chem. A* **2004**, *108*, 5299-5307.
(13) Dyke, J. M.; Levita, G.; Morris, A. Ogden, J. S.; Algarra, M.; Santos, J.P.; Dias, A. A; Costa, M. L.; Rodrigues, P.; Barros, M. T. Contrasting behavior in azide pyrolyses: An investigation of the thermal decompositions of methyl azidoformate, ethyl azidoformate and 2-azido-N, N-dimethylacetamide by ultraviolet photoelectron spectroscopy and matrix isolation infrared spectroscopy. *Chem. Eur. J.* **2005**, *11*, 1665-1676.
(14) Pinto, R. M.; Dias, A. A.; Costa, M. L.; Rodrigues, P.; Barros, M. T.; Ogden, J. S.; Dyke, J. M. Thermal Decomposition of Methyl 2-Azidopropionate Studied by UV Photoelectron Spectroscopy and Matrix Isolation IR Spectroscopy: Heterocyclic Intermediate vs Imine Formation. *J. Phys. Chem. A* **2011**, *115*, 8447-8457 (*and references therein*).
(15) Pinto, R. M.; Dias, A. A.; Levita, G.; Rodrigues, P.; Barros, M. T.; Dyke, J. M. Costa, M. L. Pyrolysis of 3-azidopropionitrile studied by UV photoelectron and matrix-

isolation IR spectroscopies: Formation of ketenimine H2C=C=NH. *J. Mol. Struct.* **2012**, *1025*, 151-159.
(16) Wentrup, C. *Azides and nitrenes. Reactivity and utility, Academic Press: Inc. Orlando, Florida, FL* **1984**.
(17) Wentrup, C. Nitrenes, Carbenes, Diradicals, and Ylides. Interconversions of Reactive Intermediates. *Acc. Chem. Res*. **2011**, *44*, 393-404.
(18) Gritsan, N. P. Study of photochemical transformations of organic azides by matrix isolation techniques and quantum chemistry. *Russ. Chem. Rev*. **2007**, *76*, 1139-1160.
(19) Kubicki, J.; Luk, H. L.; Zhang, Y.; Vyas, S.; Peng, H. L.; Hadad, C. M.; Platz, M. S. Direct Observation of a Sulfonyl Azide Excited State and Its Decay Processes by Ultrafast Time-Resolved IR Spectroscopy. *J. Am. Chem. Soc*. **2012**, *134*, 7036-7044.
(20) Jarvis, B.B.; Nicholas, P.E.; Midiwo, J. O. Thermolysis of alpha-azido Sulfides, sulfoxides, and sulfones - Dependence of Mechanism on Oxidation-state of Sulfur. *J. Am. Chem. Soc*. **1981**, *103*, 3878-3882.
(21) Nicewicz, D. A.; MacMillan, D. W. C. Merging photoredox catalysis with organocatalysis: The direct asymmetric alkylation of aldehydes. *Science* **2008**, *322*, 77-80.
(22) Chen, R. T.; Marchesan, S.; Evans, R. A.; Styan, K. E.; Such, G. K.; Postma, A.; McLean, K. M.; Muir, B. W.; Caruso, F. Photoinitiated Alkyne-Azide Click and Radical Cross-Linking Reactions for the Patterning of PEG Hydrogels. *Biomacromolecules* **2012**, *13*, 889-895.
(23) Arumugam, S.; Orski, S.V.; Loclin, J.; Popik, V. V. Photoreactive Polymer Brushes for High-Density Patterned Surface Derivatization Using a Diels-Alder Photoclick Reaction. *J. Am. Chem. Soc.* **2012**, *134*, 179-182.
(24) Bharatam, P. V.; Kaur. A.; Kaur. D. Electronic structure of N-sulfenylimines. *J. Phys. Org. Chem.* **2003**, *16*, 183-188.
(25) Bharatam, P. V. Moudgil, R. Kaur, D. Se-N interactions in selenohydroxylamine: a theoretical study. *J. Chem. Soc., Perkin Trans.* **2000**, *2*, 2469-2474.
(26) Esteban, J.; Costa, A. M.; Urpí, F.; Vilarrasa, J. From (E)- and (Z)-ketoximes to N-sulfenylimines, ketimines or ketones at will. Application to erythromycin derivatives. *Tetrahedron Lett.* **2004**, 45, 5563-5567.
(27) Lamy, E.; Lüthi, P.; Paturel, C.; Winkler, T.; Jung, P. M. J. Synthesis and reactivity of 4 "-phenylsulfinimine-avermectin B-1 and 4 '-phenylsulfinimine-avermectin B-1 monosaccharide derivative. *Tetrahedron Lett.* **2006**, *47*, 5657-5660.
(28) Quinto-Hernandez, A.; Wodtke, A. M.; Bennett, C. J.; Kim, Y. S.; Kaiser, R I. On the Interaction of Methyl Azide (CH3N3) Ices with Ionizing Radiation: Formation of Methanimine (CH2NH), Hydrogen Cyanide (HCN), and Hydrogen Isocyanide (HNC). *J. Phys. Chem. A* **2011**, *115*, 250-264.
(29) Khlifi, M.; Paillous, P.; Bruston, P.; Raulin, F.; Guillemin, J. C. Absolute IR band intensities of CH_2N_2, CH_3N_3, and CH_3NC in the 250-4300 cm^{-1} region and upper limits of abundance in Titan's stratosphere. *Icarus* **1996**, *124*, 318-328.
(30) Frankowski, M.; Fox, B. S.; Smith-Gicklhorn, A. M.; Beyer, M. K.; Bondybey, V. E.; Algarra, M.; Costa, M. L.; Rodrigues, P.; Barros, M. T.; Cordeiro, M. N. D. S. Matrix-isolation FTIR study of azidoacetone and azidoacetonitrile. *Low Temperature Phys*. **2003**, *29*, 870-875.

(31) Theulé, P.; Borget, F.; Mispelaer, F.; Danger, G.; Duvernay, F.; Guillemin, J. C.; Chiavassa. T. Hydrogenation of solid hydrogen cyanide HCN and methanimine CH_2NH at low temperature. *Astron. Astrophys.* **2011**, *534*, A64
(32) Jacox, M. E.; Milligan, D. E. The Infrared Spectrum of Methylenimine. *J. Mol. Spec*. **1975**, *56*, 333-356.
(33) Hamada, Y.; Hashiguchi, K.; Tsuboi, M.; Koga, Y.; Kondo, S. Pyrolysis of Amines: Infrared Spectrum of Methyleneimine. *J. Mol. Spec.* **1984**, *105*, 70-80.
(34) Roos B. O. The Complete Active Space Self-Consistent Field Method and Its Applications in Electronic Structure Calculations. In Advances in Chemical Physics; Ab Initio Methods in Quantum Chemistry II, ed. Lawley, K. P. John Wiley & Sons, Chichester, England, **2007**, ch. 69, p. 399.
(35) Finley, J.; Malmqvist, P. Å.; Roos, B. O.; Serrano-Andrés, L. The multi-state CASPT2 method. *Chem. Phys. Lett.* **1998**, *288*, 299-306.
(36) Roos, B. O.; Lindh, R.; Malmqvist, P.-Å.; Veryazov, V.; Widmark, P. O. Main group atoms and dimers studied with a new relativistic ANO basis set. *J. Phys. Chem. A* **2004**, *108*, 2851–2858.
(37) Roos, B. O.; Lindh, R.; Malmqvist, P. Å.; Veryazov, V.; Widmark, P. O. New relativistic ANO basis sets for transition metal atoms. *J. Phys. Chem. A* **2005**, *109*, 6575-6579.
(38) MOLCAS 8.2 (a) Veryazov, V.; Widmark, P. O.; Serrano- Andrés, L.; Lindh R.; Roos, B. O. *Int. J. Quantum Chem.* **2004**, *100*, 626-635.; (b) Aquilante, F.; Autschbach, J.; Carlson, R. K.; Chibotaru, L. F.; Delcey, M. G.; De Vico, L.; Galván, I. F.; Ferré, N.; Frutos, L. M.; Gagliardi, L.; Garavelli, M.; Giussani A.; Hoyer C. E.; Li Manni G.; Lischka, H.; Ma, D.; Malmqvist, P. Å.; Müller, T.; Nenov, A.; Olivucci, M.; Pedersen, T. B.; Peng, D.; Plasser, F.; Pritchard, B.; Reiher, M.; Rivalta, I.; Schapiro, I.; Segarra-Martí, J.; 2, Stenrup. M.; Truhlar, D. G.; Ungur, L.; Valentini, A.; Vancoillie, S.; Veryazov, V.; Vysotskiy, V. P.; Weingart, O.; Zapata, F.; Lindh, R. Molcas8: New capabilities for multiconfigurational quantum chemical calculations across the periodic table. *J. Comput. Chem.* **2016**, *37*, 506-541.
(39) Gritsan, N. P.; Platz, M. S. Kinetics, Spectroscopy, and Computational Chemistry of Arylnitrenes. *Chem. Rev.* **2006**, *106*, 3844-3867.
(40) Soto, J.; Otero, J. C.; Ávila, F. J.; Peláez, D. Conical intersections and intersystem crossings explain product formation in photochemical reactions of aryl azides. *Phys. Chem. Chem. Phys.* **2019**, *21*, 2389-2396.
(41) Aranda, D.; Ávila, F. J.; López-Tocón, I.; Arenas, J. F.; Otero, J. C.; Soto, J. An MS-CASPT2 study of the photodecomposition of 4-methoxyphenyl azide: role of internal conversion and intersystem crossing. *Phys. Chem. Chem. Phys.* **2018**, *20*, 7764-7771.
(42) Soto, J.; Otero, J. C. Conservation of El-Sayed's Rules in the Photolysis of Phenyl Azide: Two Independent Decomposition Doorways for Alternate Direc Formation of Triplet and Singlet Phenylnitrene. *J. Phys. Chem. A* **2019**, *123*, 9053-9060.
(43) Soto, J.; Rosas, J. M.; Otero, J. C.; Rodriguez-Mirasol, J.; Cordero, T. Reaction Mechanisms of 2-Butanol Dehydration over a Phosphorus-Containing Activated Carbon Acid Catalyst. *J. Phys. Chem. C* **2018**, *122*, 16772-16778.

(44) Soto, J.; Peláez, D.; Otero, J. C.; Ávila, F. J.; Arenas, J. F. Photodissociation Mechanism of Methyl Nitrate. A study with the Multi-state Second-Order Multiconfigurational Perturbation Theory. *Phys. Chem. Chem. Phys.* **2009**, *11*, 2631-2639.
(45) Peláez, D.; Arenas, J. F.; Otero, J. C.; Soto, J. Dependence of N-nitrosodimethylamine Photodecomposition on the Irradiation wavelength: Excitation to the S-2 state as a Doorway to the Dimethylamine Radical Ground-State Chemistry. *J. Org. Chem*. **2007**, *72*, 4741-4749.
(46) Ruano, C.; Otero, J. C.; Arenas, J. F.; Soto, J. Multiconfigurational Second-order Perturbation Study of the Photochem-ical Decomposition of Methyl Thionitrite. *Chem. Phys. Lett.* **2012**, *553*, 17-20.
(47) Soto J.; Imbarack, E.; López-Tocón, I.; Sanchez-Cortes, S.; Otero, J. C.; Leyton, P. Application of Surface-Enhanced Resonance Raman Scattering (SERS) to the Study of Organic Functional Materials: Electronic Structure and Charge Transfer Properties of 9,10-bis((E)-2-(pyridin-4-yl)vinyl) An-thracene. *RSC Adv.* **2019**, *9*, 14511-14519.
(48) Peláez, D.; Arenas, J. F.; Otero, J. C.; Soto, J. A complete active space self-consistent field study of the photochemistry of nitrosamine. *J. Chem. Phys*. **2006**, *125*, 164311
(49) Peláez, D.; Arenas, J. F.; Otero, J. C.; Avila, F. J.; Soto, J. Photochemistry of protonated nitrosamine: Chemical inertia of NH(2)NOH(+) versus reactivity of NH(3)NO(+). *J. Phys. Chem. A* **2008**, *112*, 8394-8402.
(50) Algarra, M.; Moreno, V.; Lazaro-Martinez, J. M.; Rodriguez-Castellon, E.; Soto, J.; Morales, Julian; Benitez, A. Insights into the formation of N doped 3D-graphene quantum dots. Spectroscopic and computational approach. *J. Colloid Interface Sci.* **2020**, *561*, 678-686.
(51) Arenas, J. F.; Otero, J. C.; Peláez, D.; Soto, J.; Serrano-Andrés, L. Multiconfigurational second-order perturbation study of the decomposition of the radical anion of nitromethane. *J. Chem. Phys.* **2004**, *121*, 4127-4132.
(52) Galván, I. F.; Delcey, M. G.; Pedersen, T. B.; Aquilante, F.; Lindh, R. Analytical State-Average Complete-Active-Space Self-Consistent Field Nonadiabatic Coupling Vectors: Implementation with Density-Fitted Two Electron Integrals and Application to Conical Intersections. *J. Chem. Theory Comput.* **2016**, *12*, 3636-3653.
(53) Arenas, J. F.; Marcos, J. I.; Otero, J. C.; Sánchez-Gálvez A.; Soto, J. A multiconfigurational self-consistent field study of the thermal decomposition of methyl azide. *J. Chem. Phys.* **1999**, *111*, 551-561.
(54) Arenas, J. F.; Marcos, J. I.; López-Tocón, I.; Otero J. C.; Soto, J. Potential-energy surfaces related to the thermal decomposition of ethyl azide: The role of intersystem crossings. *J. Chem. Phys*. **2000**, *113*, 2282-2289.
(55) Arenas, J. F.; Marcos, J. I.; Otero, J. C.; López-Tocón, I.; Soto, J. Nitrenes as intermediates in the thermal decomposition of aliphatic azides. *Int. J. Quantum Chem.* **2001**, *84*, 241-248.
(56) Wentrup, C.; Lüerssen, H.; Santos Silva, H.; Dargelos, A.; Bégué, D. Trimethylsilylnitrene and Its Surprising Rearrangement to N-(Dimethylsilyl)methanimine via Silaziridine and Silaazomethine Ylide. *Chem. Eur. J.* **2018**, *24*, 14547-14553.

(57) Yang, Y.; Deng, G.; Lu, Y.; Liu, Q.; Abe, M.; Zeng, X. Photodecomposition of Thienylsulfonyl Azides: Generation and Spectroscopic Characterization of Triplet Thienylsulfonyl Nitrenes and 3-Thienylnitrene. *J. Phys. Chem. A* **2019**, *123*, 9311-9320.
(58) Korchagin, D. V.; Akimov, A. V.; Savitsky, A.; Chapyshev, S. V.; Aldoshin, S. M.; Misochko, E. Ya. Steric Heavy Atom Effect on Magnetic Anisotropy of Triplet Tribromophenyl Nitrenes. *J. Phys. Chem. A* **2018**, *122*, 8931-8937.
(59) Yarkony, D. R. Theoretical Studies of Spin-Forbidden Radiationless Decay in Polyatomic Systems: Insights from Recently Developed Compu-tational Methods. *J. Am. Chem. Soc.* **1992**, *114*, 5406-5411.
(60) Kubicki, J.; Zhang, Y.; Vyas, S.; Burdzinski, G.; Luk, H. L.; Wang, J.; Xue, J. D.; Peng, H. L.; Pritchina, E. A.; Sliwa, M.; Buntinx, G.; Gritsan, N. P.; Hadad, C. M.; Platz, M. S. Photochemistry of 2-Naphthoyl Azide. An Ultrafast Time-Resolved UVVis and IR Spectroscopic and Computational Study. *J. Am. Chem. Soc.* **2011**, *133*, 9751-9761.
(61) Wan, H.; Xu, J.; Liu, Q.; Li, H.; Lu, Y.; Abe, M.; Zeng, X. Contrasting Photolytic and Thermal Decomposition of Phenyl Azidoformate: The Curtius Rearrangement Versus Intramolecular C-H Amination. *J. Phys. Chem. A* **2017**, *121*, 8604-8613.
(62) Beǵué, D.; Santos-Silva, H.; Dargelos, A.; Wentrup, C. Imidoylnitrenes R'C(=NR)-N, Nitrile Imines, 1*H*-Diazirines, and Carbodiimides: Interconversions and Rearrangements, Structures, and Energies at DFT and CASPT2 Levels of Theory. *J. Phys. Chem. A* **2017**, *121*, 8227-8235.
(63) Deng, G.; Dong, X.; Liu, Q.; Li, D.; Li, H.; Sun, Q.; Zeng, X. The decomposition of benzenesulfonyl azide: a matrix isolation and computational study. *Phys. Chem. Chem. Phys.* **2017** *19*, 3792-3799.
(64) Peng, X. L.; Ding, W. L.; Li, Q. S.; Li, Z. S. Theoretical insights into photo-induced Curtius rearrangement of chlorodifluoroacetyl azide. *Org. Chem. Front*. **2017**, *4*, 1153-1161.
(65) Xie, B. B.; Cui, C. X.; Fang, W. H.; Cui, G. Photoinduced Curtius rearrangements of fluorocarbonyl azide, $FC(O)N_3$: a QM/MM nonadiabatic dynamics simulation. *Phys. Chem. Chem. Phys.* **2018**, *20*, 19363-19372.
(66) Du, L.; Qiu, Y.; Lan, X.; Zhu, R.; Phillips, D. L.; M.-D.; Li, M.-D.; Dutton, A. S.; Winter, A. H. Direct Detection of the Open-Shell Singlet Phenyloxenium Ion: An Atom-Centered Diradical Reacts as an Electrophile. *J. Am. Chem. Soc.* **2017**, *139*, 15054-15059.
(67) Fernández -Ramos, A.; Rodriguez-Otero, J.; Rios, M. A.; Soto, J. Intramolecular proton transfer in 2-(2 '-hydroxyphenyl)benzoxazole: the reliability of ab initio calculations on simplified structures. *J. Mol. Struct.* (Theochem) **1999**, *489*, 255-262.
(68) Dong, X.; Deng, G.; Xu, J.; Li, H.; Zeng, X. Decomposition of Sulfonyl Azide Isocyanate and Sulfonyl Diazide: The Oxygen-Shifted Curtius Rearrangement via Sulfonyl Nitrenes. *J. Phys. Chem. A* **2018**, *122*, 8511-8519.
(69) Lieber, E.; Rao, C. N. R.; Thomas, A. E.; Oftedahl, E., Minnis, R.; Nambury, C. V. N. Infrared Spectra of Acides, Carbamyl Azides and Other Azido Derivatives - Anomalous Splittings of the N-3 Stretching Bands. *Spectrochim. Acta* **1963**, *19*, 1135-1144.
(70) Böhme, H; Morf, D. Uber Alpha-Azido-Thioather und Alpha-Azido-Sulfone. *Chem. Ber.* **1957**, *90*, 446-450

(71) Shen, T.; Huang X.; Liang Y.F.; Jiao N. Cu-Catalyzed Transformation of Alkynes and Alkenes with Azide and Dimethyl Sulfoxide Reagents. *Org. Lett.* **2015**, *17*, 6186-6189
(72) Borget, F.; Chiavassa, T.; Aycard, J. P. Photoreactivity on a water ice surface: cyanoacetylene (HC_3N) reaction with atomic oxygen issued from the photodissociation of ozone (O(3)) at 255 nm. *Chem. Phys. Lett*. **2001**, *348*, 425-432.
(73) Heß, B. A.; Marian, C. M.; Wahlgren U.; Gropen, O. A mean-field spin-orbit method applicable to correlated wavefunctions. *Chem. Phys. Lett.* **1996**, *251*, 365-371.
(74) Malmqvist, P.Å.; Roos B. O.; Schimmelpfenning, B. The restricted active space (RAS) state interaction approach with spin-orbit coupling. *Chem. Phys. Lett.* **2002**, *357*, 230-240.
(75) Ribbing, C.; Gilliams, B.; Pierloot, K.; Roos B. O.; Karlström, G. The optical absorption spectrum of the octahedral RhCl63- complex: Ab initio calculations of excitation energies and the effect of spin-orbit coupling. *J. Chem. Phys.* **1998**, *109*, 3145-3152.
(76) Arenas, J. F.; Otero, J. C.; Peláez, D.; Soto, J. Photodissociation mechanism of nitramide: A CAS-SCF and MS-CASPT2 study. *J. Phys. Chem. A* **2005**, *109*, 7172-7180.
(77) Arenas, J. F.; Otero, J. C.; Peláez, D.; Soto, J. The ground and excited state potential energy surfaces of nitromethane related to its dissociation dynamics after excitation at 193 nm. *J. Chem. Phys.* **2003**, *119*, 7814-7823.
(78) Soto, J.; Ávila, F. J.; Otero, J. C. Arenas, J. F. Comment on "Multiconfigurational perturbation theory can predict a false ground state" by C. Camacho, R. Cimiraglia and H. A. Witek. *Phys. Chem. Chem. Phys*. **2011**, *13*, 7230-72131.
(79) Arenas, J. F.; López-Tocón, I.; Otero J. C.; Soto, J. Carbene Formation in its Lower Singlet State from Photoexcited 3H-diazirine or Diazomethane. A Combined CASPT2 and Ab Initio Direct Dynamics Trajectory Study. *J. Am. Chem. Soc.* **2002**, *124*, 1728-1735.
(80) Bernardi, F.; Olivucci, M.; Robb, M. A.; Vreven T.; Soto, J. An Ab Initio study of the Photochemical Decomposition of 3,3-dimethyldiazirine. *J. Org. Chem.* **2000**, *65*, 7847-7857.
(81) Allouche, A. R. Gabedit - A graphical user interface for computational chemistry softwares. *J. Comput. Chem.* **2011**, *32*, 174-183.
(82) Schaftenaar G.; Noordik, J. H. J. Molden: a pre- and post-processing program for molecular and electronic structures. *J. Comput. Aided Mol. Design.* **2000**, *14*, 123-134.
(83) Bode B. M.; Gordon, M. S. MacMolPlt: A graphical user interface for GAMESS. *J. Mol. Graphics Modell*. **1998**, *16*, 133-138.
(84) Pulay, P.; Fogarasi, G.; Pang, F.; Boggs, J. E. Systematic ab Initio Gradient Calculation of Molecular Geometries, Force Constants, and Dipole Moment Derivatives. *J. Am. Chem. Soc*. **1979**, *101*, 2550-3560.
(85) Wilson, Jr. E. B.; Decius, J. C.; Cross, P. C. in Molecular Vibrations, MacGraw Hill, New York, USA, **1955**.
(86) Keresztury, G.; Jalsovszky, G. Alternative calculation of vibrational potential energy distribution. *J. Mol. Struct*. **1971**, *10*, 304-305.
(87) Arenas, J. F.; Centeno, S. P.; Marcos, J. I.; Otero, J. C.; Soto, J. A method to improve the agreement between calculated and observed vibrational frequencies after scaling of a quantum mechanical force field. *J. Chem. Phys.* **2000**, *113*, 8472-8477.

(88) Arenas, J. F.; Sánchez-Gálvez, A.; Otero, J. C.; Soto, J. Standard procedure to obtain a convenient set of scale factors in the SQMFF method. *J. Mol. Struct.* **1996**, *385*, 49-54.
(89) Lee, C.; Yang, W.; Parr, R. G. Development of the Colle-Salvetti Correlation-Energy Formula into a Functional of the Electron-Density. *Phys. Rev. B* **1988**, *37*, 785-789.
(90) Becke, A. D. Density-Functional Exchange-Energy Approximation with Correct Asymptotic-Behavior. *Phys. Rev. A* **1988**, *38*, 3098-3100.
(91) Ditchfield, R.; Hehre, W. J.; Pople, J. A. Self-Consistent Molecular Orbital Methods. IX. Extended Gaussian-type basis for molecular-orbital studies of organic molecules. *J. Chem. Phys.* **1971**, *54*, 724-729
(92) Møller, C.; Plesset, M. S. Note on an approximation treatment for many-electron systems. *Phys. Rev.* **1934**, *46*, 618-622.
(93) Weigend F. Accurate Coulomb-fitting basis sets for H to Rn. *Phys. Chem. Chem. Phys.* **2006**, *8*, 1057-1065.
(94) Weigend F.; Ahlrichs, R. Balanced basis sets of split valence, triple zeta valence and quadruple zeta valence quality for H to Rn: Design and assessment of accuracy. *Phys. Chem. Chem. Phys.* **2005**, *7*, 3297-3305.
(95) Frisch, M. J.; Trucks, G. W.; Schlegel, H. B.; Scuseria, G. E.; Robb, M. A.; Cheeseman, J. R.; Scalmani, G.; Barone, V.; Petersson, G. A.; Nakatsuji, H.; Li, X.; Caricato, M.; Marenich, A. V.; Bloino, J.; Janesko, B. G.; Gomperts, R.; Mennucci, B.; Hratchian, H. P.; Ortiz, J. V.; Izmaylov, A. F.; Sonnenberg, J. L.; Williams-Young, D.; Ding, F.; Lipparini, F.; Egidi, F.; Goings, J.; Peng, B.; Petrone, A.; Henderson, T.; Ranasinghe, D.; Zakrzewski, V. G.; Gao, J.; Rega, N.; Zheng, G.; Liang, W.; Hada, M.; Ehara, M.; Toyota, K.; Fukuda, R.; Hasegawa, J.; Ishida, M.; Nakajima, T.; Honda, Y.; Kitao, O.; Nakai, H.; Vreven, T.; Throssell, K.; Montgomery, J. A., Jr.; Peralta, J. E.; Ogliaro, F.; Bearpark, M. J.; Heyd, J. J.; Brothers, E. N.; Kudin, K. N.; Staroverov, V. N.; Keith, T. A.; Kobayashi, R.; Normand, J.; Raghavachari, K.; Rendell, A. P.; Burant, J. C.; Iyengar, S. S.; Tomasi, J.; Cossi, M.; Millam, J. M.; Klene, M.; Adamo, C.; Cammi, R.; Ochterski, J. W.; Martin, R. L.; Morokuma, K.; Farkas, O.; Foresman, J. B.; Fox, D. J. Gaussian, Inc *Gaussian 16, Revision A.03*, Gaussian Inc.: Wallingford CT, **2016**.

Table of Contents

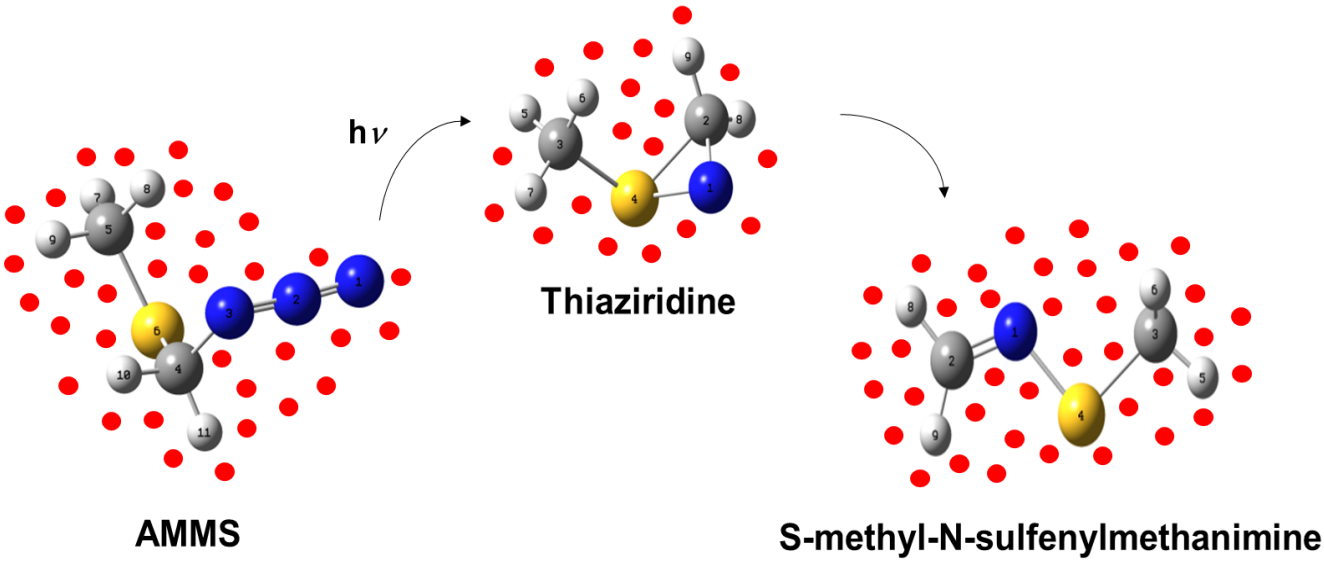

Matrix isolation FTIR and MS-CASPT2 studies of the photo decomposition of azidomethyl methyl sulfide (AMMS) in Ar (●) matrix at 10K: a S_2/S_1 conical intersection on the nitrene potential energy surfaces explains the formation of ***S-methyl-N-sulfenyl-methanimine***.